Three-dimensional noble-metal nanostructure: A new kind of substrate for sensitive, uniform, and reproducible surface-enhanced Raman scattering

2014 Chinese Phys. B 23 087801

(http://iopscience.iop.org/1674-1056/23/8/087801)

INVITED REVIEW — International Conference on Nanoscience and Technology, China 2013

Three-dimensional noble-metal nanostructure: A new kind of substrate for sensitive, uniform, and reproducible surface-enhanced Raman scattering*

Tian Cui-Feng(田翠锋)[a)b)], You Hong-Jun(尤红军)[a)†], and Fang Ji-Xiang(方吉祥)[a)‡]

[a)] *State Key Laboratory for Mechanical Behavior of Materials, School of Science, Xi'an Jiaotong University, Xi'an* 710049, *China*
[b)] *Department of Physics, Shanxi Datong University, Datong* 037009, *China*

(Received 4 September 2013; revised manuscript received 30 April 2014; published online 10 June 2014)

Surface-enhanced Raman spectroscopy (SERS) is a powerful vibrational spectroscopy technique for highly sensitive structural detection of low concentration analyte. The SERS activities largely depend on the topography of the substrate. In this review, we summarize the recent progress in SERS substrate, especially focusing on the three-dimensional (3D) noble-metal substrate with hierarchical nanostructure. Firstly, we introduce the background and general mechanism of 3D hierarchical SERS nanostructures. Then, a systematic overview on the fabrication, growth mechanism, and SERS property of various noble-metal substrates with 3D hierarchical nanostructures is presented. Finally, the applications of 3D hierarchical nanostructures as SERS substrates in many fields are discussed.

Keywords: surface-enhanced Raman spectroscopy, noble metal, hierarchical nanostructure, FDTD

PACS: 78.30.−j, 78.67.Pt, 62.23.St, 47.11.Fg **DOI:** 10.1088/1674-1056/23/8/087801

1. Introduction

Surface-enhanced Raman spectroscopy (SERS) as a powerful technique has enormous potential applications in biochemistry, chemical production, and environmental monitoring.[1–3] SERS allows the highly sensitive structural detection of low concentration analyte through the amplification of electromagnetic field generated by the excitation of localized surface plasmons.[4,5] The SERS mechanism was discovered by Jeanmaire and Vanduyne in 1977.[6] They found that the intensity of Raman spectrum could be greatly enhanced when the analyte molecules were located on a rough metal substrate and the enhancement factor is highly dependent on the surface structure.

Two kinds of enhancement mechanisms are involved for SERS. One is the chemical enhancement caused by the charge transfer between the metal surface and the adsorbed analyte molecules.[7] The other is the local electromagnetic enhancement that originates from the excitation of the collective oscillations of free electrons in noble or transition metals, which is termed physical enhancement.[8–10] Usually, the physical enhancement is much higher than the chemical enhancement, and much more attention is paid to the structures that offer obvious physical enhancements. The physical enhancement is mainly due to electromagnetic enhancement from localized plasmon resonances in noble or transition metals.[10,11] The plasmonic coupling effect induces very high local electromagnetic enhancement in certain regions called 'hot spots', leading to high SERS enhancement (more than 10^{10}) that even allows single molecule detection.[12,13]

The intensity of local electric field can be promoted by two kinds of nanostructures on the SERS substrates. One is a sharp tip with high curvature that acts as a 'lightning rod', and the other is a slit formed between neighboring metal nanoparticles that serve as a nanogap. These two kinds of structure-determined enhancements come from the 'lightning rod' and nanogap enhancement mechanisms.[14–16] Finite-difference time-domain (FDTD) simulations reveal that the local electric fields at the tips and slit will be greatly magnified by the surface plasmon resonance.[17–19] The SERS substrates containing these two kinds of structures have been widely prepared.

According to the morphologies, the SERS substrates can be classified into three classes in general. The first one is a bulk substrate which is prepared using 'top–down' methods, such as electron beam lithography, nanosphere lithography, and electrospinning technique.[20–23] At present, these techniques still have difficulties in creating highly dense and fine nanotips and nanogaps on the surface of the substrate.[15] Thus, only a moderate enhancement (10^5–10^6) has been obtained with this kind of substrate.[24] The second class involves metal nanoparticle colloids such as Au or Ag nanoparticles with sizes of 50 nm–100 nm. The 'hot spots' can be gen-

*Project supported by the National Natural Science Foundation of China (Grant Nos. 11304188, 51171139, and 51201122) and the Specialized Research Fund for the Doctoral Program of Higher Education, China (Grant No. 20120201120049).

†Corresponding author. E-mail: hjyou@mail.xjtu.edu.cn
‡Corresponding author. E-mail: jxfang@mail.xjtu.edu.cn

erated at the gaps between the aggregated nanoparticles.[25–27] This type of substrate is challenged by poor reproducibility.[28] By reducing the sizes of the metal nanoparticles, the density of gaps in a certain area can be increased; however, efficient SERS cannot be generated due to the small scattering cross sections.[29,30] The third class is hierarchical nanoparticles with nanogaps and nanotips built on the nanoparticle surface.[17,18,31] This substrate has generated much research interest because SERS enhancement over 10^7 has been obtained with a relatively high reproducibility.[17] Due to the abundance of bright 'hot spots' constructed on an individual hierarchical particle, the enhanced SERS signals can be obtained on a single particle substrate.[19,32] Thus, the hierarchical particles can not only be used as a single-particle SERS substrate, but also be aggregated to form particle-array SERS substrates.[33,34] As a single-particle SERS substrate, the hierarchical particles can be dispersed in solution or delivered into cells through blood flow to detect the Raman signals of molecules in solution or cells.[35–37]

Recently, various hierarchical noble-metal nanostructures as SERS substrates have been synthesized and studied. However, systematic reports are still rare. In this review, we first discuss the physical mechanism of the hierarchical nanostructures for SERS. Then, various synthesis methods, the mechanism of shape control, and SERS properties of the hierarchical nanostructures are described. Finally, the applications of the hierarchical nanostructures as SERS substrates in many fields are summarized.

2. Electromagnetic enhancement

As mentioned above, the maximal electromagnetic field is commonly located in the nanogaps or other jagged/sharp areas of the plasmonic materials. Based on the interaction theory, the gap between the two nanoparticles has been classified into three distinct regimes.[38] In the classical regime, when the space between the nanospheres is larger than 1 nm, the plasmonic coupling can be well described within classical electrodynamics, and the local electric field is suitably calculated by local model. For the crossover regime that occurs for interparticle separations below 1 nm but larger than 0.5 nm, the classical description does not hold true and quantum mechanical effects begin to play an important role in the optical response of the system. In the conductive regime, when the interparticle separation is smaller than 0.5 nm, the charge transfer plasmon and blue shift of the energy could be accurately described by the quantum mechanical approach. In this quantum area the local model must be modified with a nonlocal dielectric constant to simulate the field distribution of the larger plasmonic materials.

2.1. Local electric field

In the classical regime governed by classical electrodynamics, some optical properties of plasmonic materials could be accurately simulated to assist with the rationalization of experimental data, prediction, and the design of novel nanostructured materials. Based on the electromagnetic theory, several numerical simulation methods including Mie theory,[39] discrete dipole approximation (DDA),[40] and finite difference time domain (FDTD),[41] have been developed and widely used to model simple or complex geometrical configurations.

To explain the high sensitivity of hierarchical metal structures as SERS substrates, the maximal electric field enhancement at high-curvature sites and the high density of hot spots were estimated with FDTD. In Figs. 1(a) and 1(b), the intensity of the corrugated Ag nanowire is about 46 times higher

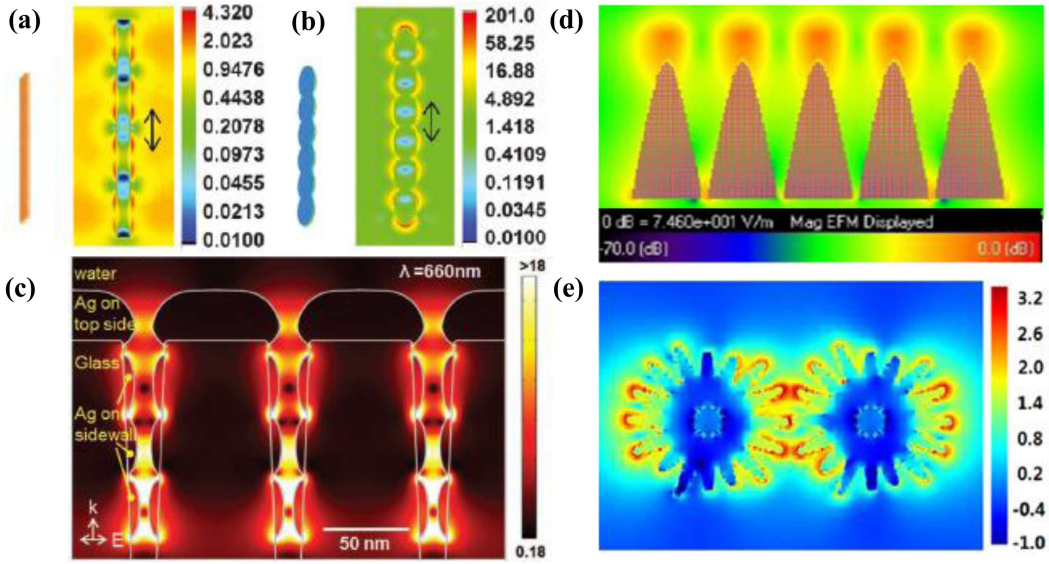

Fig. 1. The electric field distributions of (a) smooth nanowire (length = 1800 nm, width = 100 nm, height = 50 nm); (b) corrugated nanowire (total six nodes: each with long axis $D_1 = 300$ nm, short axis $D_2 = 150$ nm, joint width $D_3 = 50$ nm, and thickness $H = 50$ nm);[42] (c) nanogap-rich silver nanoislands surrounding glass nanopillars;[43] (d) the nanotips of Au flower;[44] and (e) two nanourchins with hollow Au–Ag alloy, the right color bar is the logarithmic value of the maximum field intensity.[32]

than that of the smooth Ag nanowire.[42] Furthermore, with the increase of corrugated area from two-dimensional (2D) case to three-dimensional (3D) case, the nanogap-rich silver nanoislands generate strongly localized high-density hot spots on both the top and side of glass nanopillar arrays (Fig. 1(c)).[43] If the curvature is higher, the electric field intensities at the apexes of the gold nanotips are remarkably higher (Fig. 1(d)).[44] This phenomenon can be explained by the lightning-rod effect that results in the gigantic electric field. The SERS signal of the gold nanoflowers was ~ 25 times stronger than that of spherical Au nanoparticles.[44] As the distance between the adjacent tips on the hollow Au–Ag alloy nanourchins (HAAA-Nus) decreases (Fig. 1(e)), hot spots at the sharp tips and the nanogaps between adjacent tips appear with maximal field intensities ($|E|^2 \sim 1000$).[32] It is obviously indicated that the 3D hierarchical nanostructures increase the density of hot spots and at the same time, their high curvatures improve the local electric field. They can also improve the signal uniformity over a SERS substrate, even if there is a local variation in the metal nanostructures.[45,46]

2.2. Nonlocal electric field

The local model of free electron response inside a metallic structure is successful in describing the gap whose critical dimensions are above one nanometer. However, when the interspace is below it, a more appropriate description should take into account the atomic and subatomic interactions, and electron–electron repulsion in particular. Ciracì *et al.* used the hydrodynamic model to take quantum effects into account on the assumption that the delocalization of the surface charge is a dominant process.[47] Alternative semi-empirical models have been developed that emphasize the tunneling current between the two surfaces, which is present at very small separations.[38,48] By using the quantum corrected model (QCM) simulation, the crossover is clearly seen at $d \approx 0.31$ nm (d is the distance of the two atomic force microscope (AFM) tips with gold nanoparticle).[49] The result indicates that quantum-tunneling charge transfer screens the localized plasmon surface charge, thereby reducing the enhanced fields and plasmonic coupling as well.

Therefore, within the classical regime, the hierarchical structures with uniform and abundant gaps, tips, and cavities could offer high-density hot spots and high-intensity plasmon resonances.

3. Fabrication of hierarchical noble metal

To synthesize these hierarchical structures, many diverse methods have been developed in the past ten years, including seed-mediated growth,[32] redox reactions,[17,18,31] electric deposition,[50,51] template-directed method,[52] electron-beam lithography (EBL),[53] combined methods,[54] etc. These methods and growth mechanisms are discussed below.

3.1. Seed-mediated growth

The method of seed-mediated growth is prominent for the controllability, uniformity and selectivity in sample synthesis. The nucleation and growth steps are separated so that the final morphology can be well controlled in terms of size, shape, and aspect ratio.[9,55–57]

It is possible that the resulting nanostructures are highly uniform because the narrow distribution of the seeds makes the subsequent growth of the complex nanostructures almost homogenous. If the lattice constant of the deposited metal is near that of the seeds, the crystal structure of the seed will be transferred to the product via epitaxial overgrowth. However, because of other growth factors, the resulting morphology of the nanostructure will deviate from that of the initial seed. In addition, once the seed is partially oxidized, it will be a site for new hierarchical growth, such as the synthesis of the HAAA-NUs (Fig. 2).[32] With the addition of L-Dopa, the silver ions are dissolved into the reaction solution and deoxidized. Then the Ag atom attached to the Au surface, forming an Au–Ag alloy. During the subsequent stages of reaction, the Ag seeds are further depleted and Au–Ag multiple tips are overgrown to form the sea urchin-like morphology. The HAAA-NUs (less than 100 nm) have a higher density of tips (more than 100 tips per nanourchin) than nanostars or nanoflowers.[58–60] Thus, through utilizing the method of seed-mediated growth, 3D tips of high density could be fabricated successfully. In addition, hierarchical single nanoparticles with high-density tips, such as flower-like and urchin-like particles which are illuminated below, can be prepared by using reduction method.

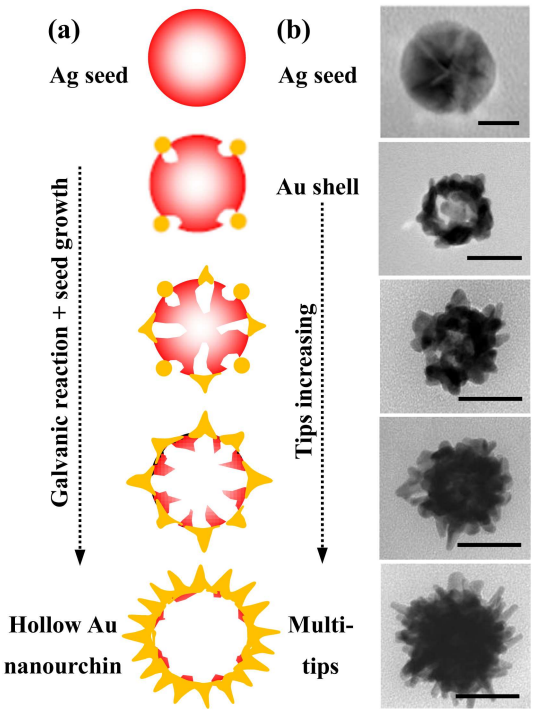

Fig. 2. (a) Scheme of the HAAA-NU particle growth from Ag seed to tip-rich nanourchin. (b) Corresponding transmission electron microscope (TEM) images. The scale bar for the Ag seed is 10 nm, and the scale bars for the others are 50 nm.[32]

3.2. Redox reaction

The redox reaction as a method of fabricating the hierarchical metal structures has many attractive characteristics including simplicity, rapidness, and rich product structure. In the reduction, metal samples with various topologies are synthesized using a metal salt and a deoxidizer. To achieve an elaborate design, some protective agents or inorganic salts are added to the reductive solution. Of course, the topology of the metal structures can be well controlled and tuned by the temperature, concentration, time or second reduction.

For example, when the temperature increases from 0 °C to 40 °C, the morphology transforms from flower-like to meatball-like shape (Fig. 3(a)).[17] At the same time, the sizes of the particles decrease accordingly. At higher temperature, the reaction speed will increase and the diffusion speed of gold atoms to the surface of the particles will be improved by a thermal driving force.[61] Thus, the anisotropic growth of the tips will be eliminated by the rapid spread of gold atoms at higher temperatures.[62] Therefore, the sharp blade-like petals will disappear at higher temperatures. By changing the concentrations of $AgNO_3$ and L-AA as well as reaction times,[18] the topographies of the obtained Ag mesoparticles can be successfully tuned from meatball-like shape to coral-like, urchin-like and highly-branched shapes (Fig. 3(b)). According to the mechanism given by LaMer and Dinegar (Fig. 3(c)),[63] the final morphology of the single noble metal particle can be well controlled by adjusting the amount of reactant, time, and the secondary growth condition. By adding the secondary amount of Fe, the growths of the atom, nuclei, and particles will occur again. However, the new Au atoms will attach onto the produced particles. The consequence is that the size and topography of Au mesoparticles can be widely tailored by controlling the amount and the time of the secondary injection of the Fe suspension as demonstrated in Fig. 3(d). The number and density of the spikes on the particles can be enhanced by increasing the amount of Fe content in the second injection.

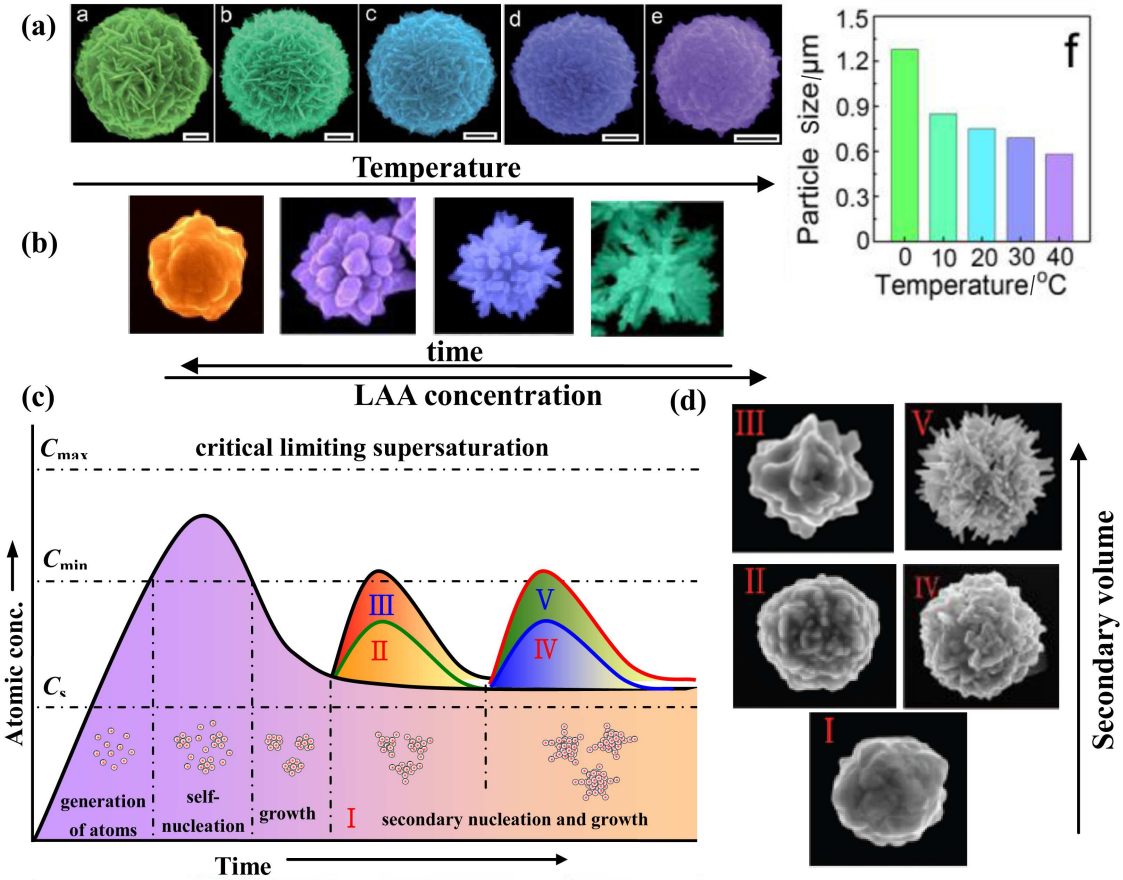

Fig. 3. Morphology transformations of hierarchical noble-metal particles under different redox reaction conditions. (a) Au mesoparticles synthesized at different temperatures: 0 °C, 10 °C, 20 °C, 30 °C, and 40 °C. The scale bar is 500 nm.[17] (b) Ag mesoparticles with tunable surface topographies produced by changing the synthesis parameters.[18] (c) Schematic plot of a gold atom concentration versus time, illustrating the growth of Au mesoparticles. (d) Au mesoparticles, types I–V, synthesized under various conditions.[31]

3.3. Electrochemical method

Some complex structures can be formed on the electrode by designing the proper potential and concentration of electrolytes or other parameters using theory from the electric double layer model.[64–67] Hierarchical morphologies including noble metal wire,[50] flower,[51] and nanoparticles on some templates can be obtained.

For Ag hierarchical wires, we analyze the changes in morphology under different reaction conditions (in Fig. 4).[50] In the electrochemical reaction solution at lower concentration of electrolyte, the thickness of the diffusion layer is larger and

the diffusion speeds of ions are slower.[65,68] Consequently, the convection has little effect on the ion diffusion. For example, in Fig. 4(a), corrugated Ag nanowires with a few nanoparticles attached are obtained using deionized water and an unusual potential (30 V). It may be that the electromigration provides the cation diffusion force and hampers the convection. Therefore, in this case, the ballistic deposition plays a more important role. As a result, the corrugated nanowires are fabricated, resulting from the high nucleation density and the flat growth front of ion flux caused by high potential. The use of low electrolyte concentrations and lower potential ($\sim$ 1 V) is insufficient to supply a diffusion force (Fig. 4(c)). This results in plate-like branches that exhibit characteristics of the diffusion limited aggregation.[69] In Fig. 4(b), the SEM image shows that the nanowires grow a lot of tiny bulges on the nanowires due to relatively sufficient mass support although a high potential is employed. In contrast, when a relatively high concentration of $AgNO_3$ solution is utilized (Fig. 4(d)), the thickness of the ion diffusion layer is small and the diffusion speed is large. Thus, the Ag nanowires have a branched morphology.

Under different conditions of electric deposition, the hierarchical nanostructures of large areas could be well controlled on the electrodes. The drawback of this method is not easy to synthesize uniform nanostructures unless it combines with other method, such as seed growth or template method.

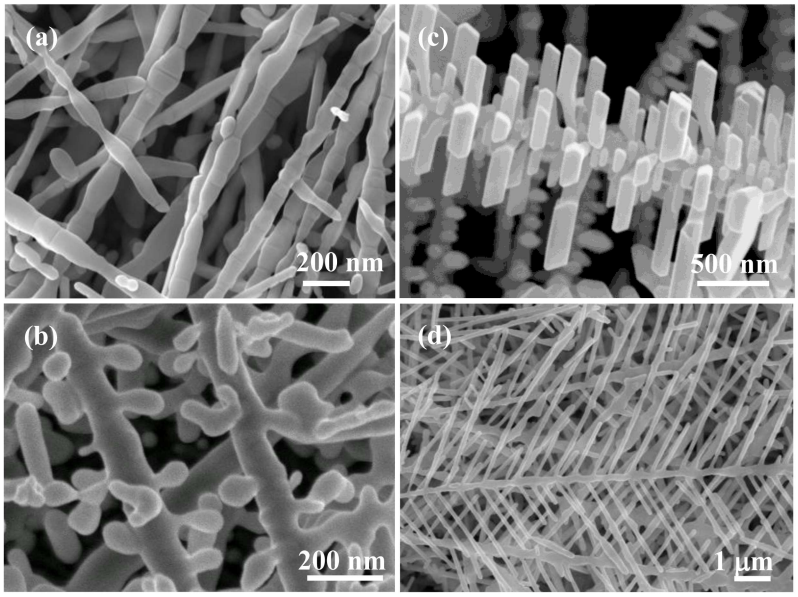

Fig. 4. Scanning electron microscope (SEM) images of the hierarchical Ag nanostructures obtained by controlling the applied potentials and concentrations of $AgNO_3$ solution in electric deposition: (a) 0 mM, 30 V; (b) 0.01 mM, 30 V; (c) 0 mM, 1 V; (d) 1 mM, 30 V.[50]

3.4. Template method

Using diverse templates to construct and control the hierarchical noble metal morphology is one of the most commonly used approaches, including solution-phase templates, porous templates, surface mask templates, organic and biologic templates, etc. In solution-phase templates, the sacrificial templates with spherical or polyhedral shapes are popular for generating extremely uniform and complex nanostructures. Fang *et al.* have obtained the silver polyhedral mesocages using Ag_2O polyhedral particle as sacrificial template (Figs. 5(a) and 5(b)).[52] Their further study found that the more uniform and deeper nanogaps can be obtained on the hollow Ag cubic particle than on single crystal Ag_2O particle by using mesocrystal Ag_2O particle as template. Accordingly, 4 times higher SERS enhancement is obtained than using single crystal Ag_2O particle as the template (Figs. 5(c) and 5(d)).[19] Another sacrificial template, cuprous oxide, can be easily synthesized to form non-spherical noble metal mesocages.[70]

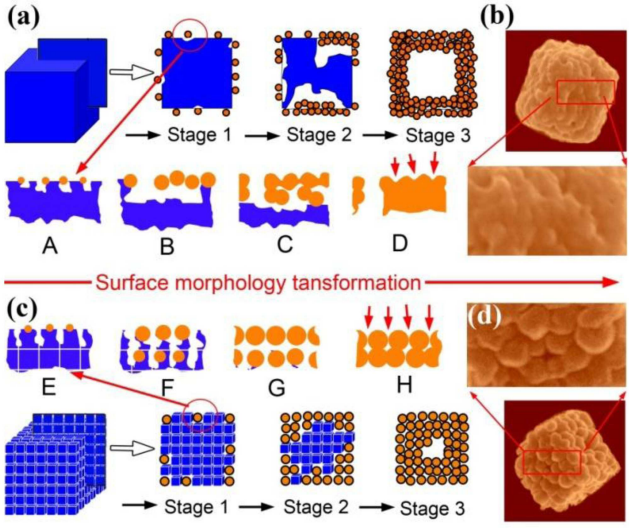

Fig. 5. Schematic diagram of the formation of Ag mesocages through the reduction of (a) single-crystal and (c) mesocrystal cubic Ag_2O particles. (b) and (d) Showing the two kinds of particles with different surface topographies.[19]

3.5. Combined method

A new route combining the above two strategies to fabricate SERS active substrates has been proposed to create high-spatial-density hot spots and simultaneously maintain reproducibility.[54,71] Normally, the periodic template is made via a top–down method and the nanostructural units are fabricated through a bottom–up method such as deposition or chemical reduction. For example, the highly homogeneous Au mesoflower arrays with smaller than 10-nm intraparticle gaps are synthesized by an *in-situ* galvanic replacement between the solution of $HAuCl_4$ and the iron substrate,[54] on which the layer of polymethylmethacrylate (PMMA) has many holes of about 300 nm–500 nm in diameter. The PMMA template is fabricated by using polymer blend lithography on an iron substrate (Fig. 6(a)).[54] Because of the unique mesostructure and uniformity, the gold mesoflower arrays demonstrate a strong and reproducible SERS enhancement (on the order of $\sim 10^7$–10^8).

In another example, electrospun nanofibrous membranes decorated with silver nanoparticles have been obtained by combining electrospinning with seed-mediated electroless plating.[72] After electrospinning the polyacrylonitrile (PAN) microfibers, the surface of the as-electrospun membranes is treated with NH_2OH creating $-C(NH_2)=N-OH$ groups. This is activated with Pd seeds (Fig. 6(b)). To construct the hierarchical SERS substrate, the processed nanofibrous membranes are attached to noble metal nanostructures by using drop-casting, electroplating, sputter-coating, and wet-chemical reaction.[73–75] The wet-chemistry reactions have several advantages because of their versatility and controllability. The Pd seeds become active sites for nucleation and growth of Ag NPs. Compared with the microspheres decorated with silver nanostructures, electrospun nanofiber-based SERS substrate has several advantages such as the flexibility, porosity, and freestanding. Obviously, the hierarchical nanostructures with large area uniformity could be constructed by this method.

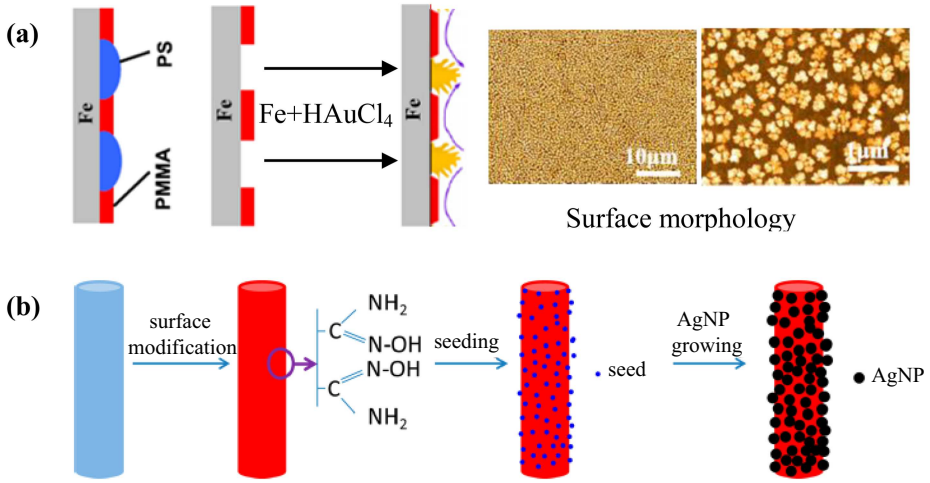

Fig. 6. A schematic diagram showing (a) the uniform gold nanoflower arrays on iron substrate with PMMA film,[54] (b) the preparation of SERS-active electrospun nanofiber surface-decorated with Ag NPs by using combined methods.[72]

4. Application of hierarchical SERS substrate

Using the above methods, various noble metal hierarchical nanostructures can be fabricated and tuned to a specific excitation wavelength. As SERS substrates, they can be widely used in the detection of organic molecules, biomarkers, and catalyzed reaction.

4.1. Detection of some organic pollutants

One of the most important applications for hierarchical noble metal SERS study is to detect some organic molecules including diethylhexyl phthalate (DEHP), pentachlorophenol (PCP), crystal violet (CV), and trinitrotoluene (TNT). Fang *et al.*[32] and Hankett *et al.*[76] have used the HAAA-NUs to detect diethylhexyl phthalate (DEHP), which has a low SERS activity and toxicity. Because of its particular structure with a high density of thorns and uniform distribution (Figs. 7(a) and 7(b)), the HAAA-NU exhibits a low stand deviation (less than 10%) of the Raman intensity (Fig. 7(c)). Furthermore, the Raman spectra of the DEHP molecule (Fig. 7(d)) can be obtained from a 785-nm excitation laser at different low concentrations. The low detection limit shows that the HAAA-NUs have a high sensitivity and can be an effective SERS substrate. Four other examples, the hierarchical mesoparticle-monolayer Au films are synthesized on a pentanol/water interface to improve uniformity and sensitivity of SERS signal.[77] From these morphologies it follows that the sea urchin-like mesostructures (Fig. 7(e)) show the highest enhancement ($\sim 10^7$–10^8) because the spike density is higher than the densities of the flower-like and meatball-like mesoparticles.

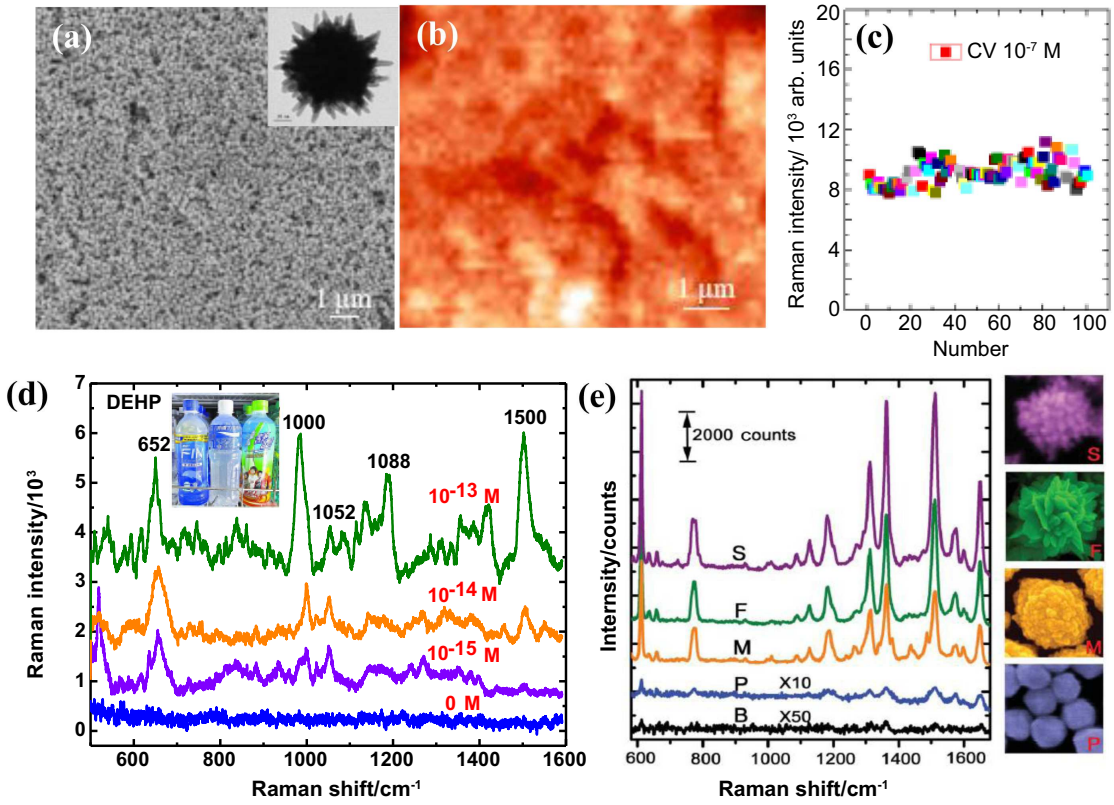

Fig. 7. (a) SEM and (b) AFM images of HAAA-NUs. (c) The Raman intensity deviations on the SERS substrate of HAAA-NUs at CV concentrations of 10^{-7} M. (d) Raman spectra of DEHP molecules obtained at 785-nm excitation laser and different concentrations of analyte.[32] (e) SERS spectrum of Rhodamine-6G (R-6G) adsorbed on the surface of the substrates with different gold mesoparticle films: sea urchin-like (S), flower-like (F), meatball-like (M), and polyhedral (P). B indicates 'background'.[77]

Although some organic molecules are strongly absorbed physically or chemically by metal surface via amine, thiol, and carboxylic acid group, there are also some organic pollutants with a low affinity to the metal surface. To combat this limitation and capture the probe molecules, the surface of noble metal has been chemically functionalized with various selective molecules such as antibodies,[78] thiolated aliphatic monolayer,[79] etc. For example, to detect trace levels of PCBs, large-scale well-separated Ag nanosheet-assembled micro-hemispheres modified with HS-β-CD is used as an effective SERS substrate.[80] An *et al.*[81] have successfully synthesized core–shell microspheres (Ag-NP coated Fe_3O_4@carbon) and used the magnetic attraction to capture the analytes. This gave high sensitivity SERS detection.

4.2. Sensor for diseases biomarkers

The hierarchical noble metal nanostructure has been utilized as an SERS sensor in testing diseases biomarkers including muramidase released protein (MRP)[82] or others and providing an efficient approach to the detecting of various diseases. Some biomarkers can indicate various cancers,[83] diabetes mellitus,[84] and viral infection.[85] For example, a 3D hierarchical plasmonic nano-architecture[86] is designed and prepared for a sensitive SERS immunosensor of protein biomarker. This SERS immunosensor exhibits a wide linear dynamic range from 0.1 pg/mL to 10 ng/mL and a low limit of detection (7 fg/mL) towards human immunoglobulin G (IgG) protein in buffer. In Fig. 8(a), the SERS intensity (at 1578 cm^{-1}) increases with increasing the IgG concentration. The Au nanostar@MGITC@SiO2, where MGITC stands for malachite green isothiocyanate particles on the Au triangle nanoarray show the strongest SERS intensity at the corresponding IgG concentration versus the Au sphere sandwich nanoparticle/Au film and the Au sphere sandwich nanoparticle/Au triangle nanoarray.

Shafer-Peltier *et al.*[87] have proposed an approach to the measuring of glucose by using SERS. The SERS-active surface used for glucose sensing is known as metal film ($\sim$ 200 nm) over nanospheres (FON) functionalized with a self-assembled monolayer (SAM) (1-decanethiol and 6-mercapto-1-hexanal) (Fig. 8(b)).[88] This DT/MH-functionalized Ag-FON sensor is used for the *in-situ* detection of glucose in a rat back. Data are collected with the conventional Raman system (Fig. 8(c)) with the rodent positioned in the place of the flow cell.[84] Figure 8(d) shows the variations of glucose concentration in the rat, measured by using SERS and the One Touch II blood glucose meter, with time. Both the standard glucose meter and the SERS-based measurements effectively track the change in glucose concentration.

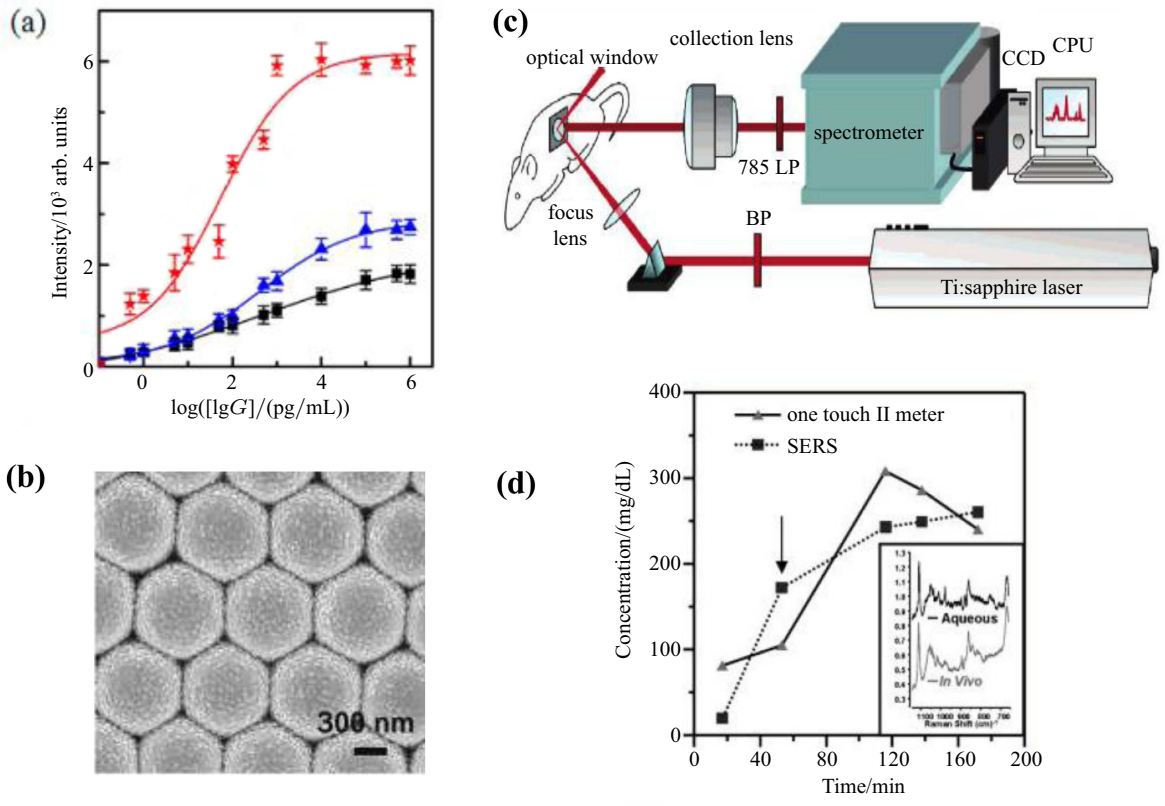

Fig. 8. (a) Plots of SERS peak intensity at 1578 cm^{-1} versus logarithmic concentration lg$G$,[86] (b) SEM image of silver film (200 nm) over 600-nm SiO_2 nanospheres.[88] (c) A rat with a surgically implanted sensor and optical window was integrated into a conventional laboratory Raman spectroscopy system. (d) Time course of the *in vivo* glucose measurement. The inset shows a typical *in vivo* spectrum compared with a typical *ex vivo* spectrum of the same surface.[84]

4.3. Monitor for catalyzed reaction

Because of high sensitivity, label free, and plasmon-driven chemical reaction, SERS can be used to monitor some chemical reactions including catalysis.[29] Classical absorption spectroscopic techniques for the study of catalytic reactions including ultraviolet-visible,[89] infrared,[90] X-ray radiation,[91] and fluorescence spectroscopy[92] are limited, owing to their disadvantages. Limited chemical information is given by UV-vis absorption spectroscopy and X-ray radiation. The main challenge in infrared spectroscopy is the competing absorption from water and spectral overlap. Fluorescent spectroscopy uses exogenous probes to measure Au-catalyzed reactions with high selectivity and sensitivity. Therefore, SERS is commonly used to detect the catalytic transformation from reagent to product. A hierarchical particle as a SERS substrate is used to monitor the catalytic reaction from p-nitrothiophenol (pNTP) dimerizing into p,p′-dimercaptoazobenzene (DMAB).[93,94] Xu *et al.*[95] used single particle SERS to investigate the surface plasmon assisted catalysis (SPAC) reactions of 4-aminothiophenol (4ATP) into and back from 4,4′-dimercaptoazobenzene (DMAB).

In Fig. 9, gold superstructures with small satellites on the surface of the ultrathin shell-coated 80-nm Au cores are used for SERS's monitoring the Au-catalyzed reduction of 4-NTP in colloidal suspension.[29] At different reaction times, the SERS signal is collected directly from the colloidal suspension to monitor the catalytic reaction (Fig. 9(a)). The characteristic SERS spectra of the 4-NTP and 4-ATP molecules are different from each other especially at 1569 cm^{-1} and 1591 cm^{-1}, respectively. It indicates that the 4-NTP molecules are converted directly into their corresponding aniline derivate 4-ATP. In Fig. 9(b), the catalytic activity of the Au satellites decreases with increasing the sizes of the Au satellites on the surface of the shell-isolated Au core. Here, the spherical core could supply more satellites (less than 10 nm) and small Au satellites increase the catalytic activity. *In-situ* SERS kinetic monitoring can also give an insight into the reaction mechanisms of heterogeneously catalyzed reactions. However, for the limit of the spatial resolution, the technology of SERS is utilized to detect the catalytic particles with dense elements.[96] Fortunately, recent advances have opened up possibilities for reducing this limitation. Combining SERS with AFM, high spectroscopic sensitivity, and nanoscale resolution make tip-enhanced Raman spectroscopy (TERS) an ideal tool to investigate and control plasmon-driven chemical reactions.[97,98]

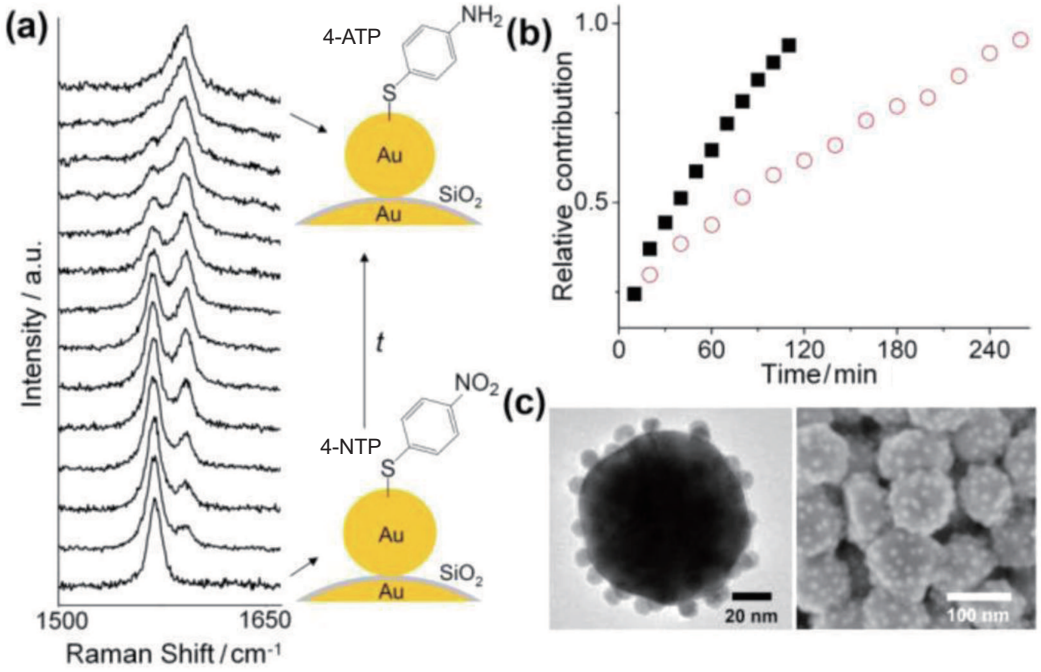

Fig. 9. (a) SERS spectra of the Au-catalyzed reduction of 4-NTP in colloidal suspension collected at different reaction times. (b) Relative contributions of 4-ATP on the surface of 5-nm (solid squars) and 10-nm (open circles) satellites versus reaction time.[29] (c) TEM and SEM images of Au superstructures with 10-nm Au satellites assembled onto an 80-nm Au core isolated by an ultrathin silica shell.

5. Conclusions

In this review, we describe recent advances in synthesizing hierarchical noble-metal nanostructure and using them as SERS substrates. First, we discuss the mechanism of electromagnetic enhancement on the hierarchical noble-metal nanostructure. The effects of localized and unlocalized electromagnetic field induced by the activated surface plasmon on the enhancement of SERS are analyzed. Second, the methods of fabricating the hierarchical noble-metal nanostructure are classified and described. Due to the anisotropic distributions of electric field and the concentration field in the electrochemical synthesis, the protrusion growth can be promoted without the help of capping agents. In some cases, the selected adsorption and self-assembly of surfactants are conducible to the formation of fine protrusions and gaps on the hierarchical nanostructure. Third, the SERS properties of various hierarchical noble-metal nanostructures and their applications are reviewed. Because of the high density of protrusions and the high density of gaps on the hierarchical nanostructure, many SERS hot spots are formed on the particle and between particles. Thus, the sensitivity, uniformity, and reproducibility of SERS signal are markedly improved. This hierarchical nanostructure SERS substrate can be widely applied to the monitoring of chemical reactions and detection of pollutants.

References

[1] Drescher D and Kneipp J 2012 *Chem. Soc. Rev.* **41** 5780
[2] Gajaraj S, Fan C, Lin M S and Hu Z Q 2013 *Environ. Monit. Assess.* **185** 5673
[3] Li Y T, Qu L L, Li D W, Song Q X, Fathi F and Long Y T 2013 *Biosens. Bioelectron.* **43** 94
[4] Li J F, Huang Y F, Ding Y, Yang Z L, Li S B, Zhou X S, Fan F R, Zhang W, Zhou Z Y, Wu D Y, Ren B, Wang Z L and Tian Z Q 2010 *Nature* **464** 392
[5] Nie S M and Emery S R 1997 *Science* **275** 1102
[6] Jeanmaire D L and Vanduyne R P 1977 *J. Electroanal. Chem.* **84** 1
[7] Sun M T, Liu S S, Chen M D and Xu H X 2009 *J. Raman Spectrosc.* **40** 137
[8] Tian Z Q, Ren B and Wu D Y 2002 *J. Phys. Chem. B* **106** 9463
[9] Xia Y N, Xiong Y J, Lim B and Skrabalak S E 2009 *Angew. Chem. Int. Ed.* **48** 60
[10] Xu H X, Aizpurua J, Kall M and Apell P 2000 *Phys. Rev. E* **62** 4318
[11] Dawson P, Duenas J A, Boyle M G, Doherty M D, Bell S E J, Kern A M, Martin O J F, Teh A S, Teo K B K and Milne W I 2011 *Nano Lett.* **11** 365
[12] Mulvihill M J, Ling X Y, Henzie J and Yang P D 2010 *J. Am. Chem. Soc.* **132** 268
[13] Rycenga M, Xia X H, Moran C H, Zhou F, Qin D, Li Z Y and Xia Y A 2011 *Angew. Chem. Int. Ed.* **50** 5473
[14] Hao F, Nehl C L, Hafner J H and Nordlander P 2007 *Nano Lett.* **7** 729
[15] Liang H Y, Li Z P, Wang W Z, Wu Y S and Xu H X 2009 *Adv. Mater.* **21** 4614
[16] Lim D K, Jeon K S, Hwang J H, Kim H, Kwon S, Suh Y D and Nam J M 2011 *Nat. Nano* **6** 452
[17] Liu Z, Zhang F, Yang Z, You H, Tian C, Li Z and Fang J 2013 *J. Mater. Chem. C* **1** 5567
[18] Cheng L, Ma C S, Yang G, You H J and Fang J X 2014 *J. Mater. Chem. A* **2** 4534
[19] Yang Z, Zhang L, You H, Li Z and Fang J 2014 *Part. Part. Syst. Charact.* **31** 390
[20] Wu W, Jung G Y, Olynick D L, Straznicky J, Li Z, Li X, Ohlberg D A A, Chen Y, Wang S Y, Liddle J A, Tong W M and Williams R S 2005 *Appl. Phys. A: Mater. Sci. Process.* **80** 1173
[21] Bellessa J, Symonds C, Vynck K, Lemaitre A, Brioude A, Beaur L, Plenet J C, Viste P, Felbacq D, Cambril E and Valvin P 2009 *Phys. Rev. B* **80** 033303

[22] Sakamoto S, Philippe L, Bechelany M, Michler J, Asoh H and Ono S 2008 *Nanotechnology* **19** 405304
[23] Cao C, Zhang J, Wen X, Dodson S L, Dao N T, Wong L M, Wang S, Li S, Phan A T and Xiong Q 2013 *ACS Nano* **7** 7583
[24] Haynes C L, McFarland A D and Van Duyne R P 2005 *Anal. Chem.* **77** 338A
[25] Gong X, Bao Y, Qiu C and Jiang C Y 2012 *Chem. Commun.* **48** 7003
[26] Le F, Brandl D W, Urzhumov Y A, Wang H, Kundu J, Halas N J, Aizpurua J and Nordlander P 2008 *ACS Nano* **2** 707
[27] Graham D, Thompson D G, Smith W E and Faulds K 2008 *Nat. Nanotechnol.* **3** 548
[28] Fang Y, Seong N H and Dlott D D 2008 *Science* **321** 388
[29] Xie W, Walkenfort B and Schlucker S 2013 *J. Am. Chem. Soc.* **135** 1657
[30] Krug J T, Wang G D, Emory S R and Nie S 1999 *J. Am. Chem. Soc.* **121** 9208
[31] Fang J X, Du S Y, Lebedkin S, Li Z Y, Kruk R, Kappes M and Hahn H 2010 *Nano Lett.* **10** 5006
[32] Liu Z, Yang Z, Peng B, Cao C, Zhang C, You H, Xiong Q, Li Z and Fang J 2014 *Adv. Mater.* **26** 2431
[33] Peng B, Li G, Li D, Dodson S, Zhang Q, Zhang J, Lee Y H, Demir H V, Yi L X and Xiong Q 2013 *ACS Nano* **7** 5993
[34] Qu L L, Li D W, Xue J Q, Zhai W L, Fossey J S and Long Y T 2012 *Lab Chip* **12** 876
[35] Qian X M, Peng X H, Ansari D O, Yin-Goen Q, Chen G Z, Shin D M, Yang L, Young A N, Wang M D and Nie S M 2008 *Nat. Biotechnol.* **26** 83
[36] Rodríuez-Lorenzo L, Álvarez-Puebla R N A, Pastoriza-Santos I, Mazzucco S, Stéphan O, Kociak M, Liz-Marzán L M and García de Abajo F J 2009 *J. Am. Chem. Soc.* **131** 4616
[37] Nalbant Esenturk E and Hight Walker A R 2009 *J. Raman Spectrosc.* **40** 86
[38] Zuloaga J, Prodan E and Nordlander P 2009 *Nano Lett.* **9** 887
[39] Mie G 1908 *Ann. Phys.* **25** 377
[40] Yang W H, Schatz G C and Van Duyne R P 1995 *J. Chem. Phys.* **103** 869
[41] Bian R X, Dunn R C, Xie X S and Leung P T 1995 *Phys. Rev. Lett.* **75** 4722
[42] Tian C F, Ding C H, Liu S Y, Yang S C, Song X P, Ding B J, Li Z Y and Fang J X 2011 *ACS Nano* **5** 9442
[43] Oh Y J and Jeong K H 2012 *Adv. Mater.* **24** 2234
[44] Pradhan M, Chowdhury J, Sarkar S, Sinha A K and Pal T 2012 *J. Phys. Chem. C* **116** 24301
[45] Wang Y, Becker M, Wang L, Liu J, Scholz R, Peng J, Gösele U, Christiansen S, Kim D H and Steinhart M 2009 *Nano Lett.* **9** 2384
[46] Wu H Y and Cunningham B T 2011 *Appl. Phys. Lett.* **98** 153103
[47] Ciracì C, Hill R T, Mock J J, Urzhumov Y, Fernández-Domínguez A I, Maier S A, Pendry J B, Chilkoti A and Smith D R 2012 *Science* **337** 1072
[48] Esteban R, Borisov A G, Nordlander P and Aizpurua J 2012 *Nature Commun.* **3** 825.
[49] Savage K J, Hawkeye M M, Esteban R, Borisov A G, Aizpurua J and Baumberg J J 2012 *Nat. Biotechnol.* **491** 574
[50] Ding C H, Tian C F, Krupke R and Fang J X 2012 *CrystEngComm* **14** 875
[51] Fang J X, Yi Y, Ding B J, Song X P and 2008 *Appl. Phys. Lett.* **92** 131115
[52] Fang J X, Liu S Y and Li Z Y 2011 *Biomaterials* **32** 4877
[53] Gopinath A, Boriskina S V, Premasiri W R, Ziegler L, Reinhard B M and Negro L D 2009 *Nano Lett.* **9** 3922
[54] Tian C F, Liu Z, Jin J H, Lebedkin S, Huang C, You H J, Liu R, Wang L Q, Song X P, Ding B J, Barczewski M, Schimmel T and Fang J X 2012 *Nanotechnology* **23** 165604
[55] Zhang Q, Li W, Moran C, Chen J, Wen L P and Xia Y 2010 *J. Am. Chem. Soc.* **132** 11372
[56] Jana N R, Gearheart L and Murphy C J 2001 *Adv. Mater.* **13** 1389
[57] Pietrobon B, McEachran M and Kitaev V 2008 *ACS Nano* **3** 21
[58] Rodríguez-Lorenzo L, Rica R D L, Álvarez-Puebla R A, Liz-Marzán L M and Stevens M M 2012 *Nat. Mater.* **11** 604
[59] Sau T K, Rogach A L, Döblinger M and Feldmann J 2011 *Small* **7** 2188
[60] Wang Z D, Zhang J Q, Ekman J, Kenis P J and Lu Y 2010 *Nano Lett.* **10** 1886
[61] Peng Z M, You H J and Yang H 2010 *ACS Nano* **4** 1501
[62] You H J, Yang S H, Ding B J and Yang H 2013 *Chem. Soc. Rev.* **42** 2880
[63] LaMer V K and Dinegar R H 1950 *J. Am. Chem. Soc.* **72** 4847
[64] He R, Chen S L, Yang F and Wu B L 2006 *J. Phys. Chem. B* **110** 3262
[65] You H J, Fang J X, Chen F, Shi M, Song X P and Ding B J 2008 *J. Phys. Chem. C* **112** 16301
[66] You H J, Ding C H, Song X P, Ding B J and Fang J X 2011 *CrystEngComm* **13** 4491
[67] You H J, Fang J X, Chen F, Zhu C, Song X P and Ding B J 2008 *Chem. Phys. Lett.* **465** 131
[68] Miyashita S, Saito Y and Uwaha M J 2005 *Cryst. Growth* **283** 533
[69] Witten T A and Sander L M 1981 *Phys. Rev. Lett.* **47** 1400
[70] Fang J X, Lebedkin S, Yang S C and Hahn H 2011 *Chem. Commun.* **47** 5157
[71] Wang J J, Duan G T, Li Y, Liu G Q, Dai Z F, Zhang H W and Cai W P 2013 *Langmuir* **29** 3512
[72] Zhang L, Gong X, Bao Y, Zhao Y, Xi M, Jiang C and Fong H 2012 *Langmuir* **28** 14433
[73] He H, Cai W, Lin Y and Dai Z 2011 *Langmuir* **27** 1551
[74] Lee C H, Tian L, Abbas A, Kattumenu R and Singamaneni S 2011 *Nanotechnology* **22** 275311
[75] Carlberg B, Ye L L and Liu J H 2011 *Small* **7** 3057
[76] Hankett J M, Zhang C and Chen Z 2012 *Langmuir* **28** 4654
[77] You H J, Ji Y T, Wang L, Yang S C, Yang Z M, Fang J X, Song X P and Ding B J 2012 *J. Mater. Chem.* **22** 1998
[78] Guven B, Akgul N B, Temur E, Tamerb U and H B I 2011 *Analyst* **136** 740
[79] Jones C L, Bantz K C and Haynes C L 2009 *Anal. Bioanal. Chem.* **394** 303
[80] Zhu C H, Meng G W, Huang Q, Li Z B, Huang Z L, Wang M L and Yuan J P 2012 *J. Mater. Chem.* **22** 2271
[81] An Q, Zhang P, Li J M, Ma W F, J G, Hu J and Wang C C 2012 *Nanoscale* **4** 5210
[82] Chen K, Han H Y and Luo Z H 2012 *Analyst* **137** 1259
[83] Mohs A M, Mancini M C, Singhal S, Provenzale J M, Leyland-Jones B, Wang M D and Nie S 2010 *Anal. Chem.* **82** 9058
[84] Stuart D A, Yuen J M, Shah N, yandres O L, Yonzon C R, Glucksberg M R, Walsh J T and Van Duyne R P 2006 *Anal. Chem.* **78** 7211
[85] Shanmukh S, Jones L, Driskell J, Zhao Y P, Dluhy R and Tripp R A 2006 *Nano Lett.* **6** 2630
[86] Li M, Cushing S K, Zhang J M, Suri S, Evans R, Petros W P, Gibson L F, Ma D L, Liu Y X and Wu N Q 2013 *ACS Nano* **7** 4967
[87] Shafer-Peltier K E, Haynes C L, Glucksberg M R and Van Duyne R P 2003 *J. Am. Chem. Soc.* **125** 588
[88] Greeneltch N G, Blaber M G, Henry A I, Schatz G C and Van Duyne R P 2013 *Anal. Chem.* **85** 2297
[89] Chowdhury B, Bravo-Suarez J J, Minura N, Lu J Q, Bando K K, Tsubota S and Haruta M 2006 *J. Phys. Chem. B* **110** 22995
[90] Shinizu K, Miyamoto Y, Kawasaki T, Tanji T, Tai Y and Satsuma A 2009 *J. Phys. Chem. C* **113** 17803
[91] de Smit E, Swart I, Creemer J F, Hoveling G H, Gilles M K, Tyliszczak T, Kooyman P J, Zandbergen H W, Morin C, Weckhuysen B M and de Groot F M F 2008 *Nature* **456** 222
[92] Lu H P, Xun L Y and Xie X S 1998 *Science* **282** 1877
[93] Kang L L, Xu P, Zhang B, Tsai H H, Han X J and Wang H L 2013 *Chem. Commun.* **49** 3389
[94] You H J, Peng Z M, Wu J B and Yang H 2011 *Chem. Commun.* **47** 12595
[95] Xu P, Kang L L, Mack N H, Schanze K S, Han X J and Wang H L 2013 *Sci. Rep.* **3** 2997
[96] Weckhuysen B M 2009 *Angew. Chem. Int. Ed.* **48** 4910
[97] Sum M T, Zhang Z L, Zheng H R and Xu H X 2012 *Sci. Rep.* **2** 647
[98] Van Schrojenstein Lantman E M, Deckert-Gaudig T, Mank A J, Deckert V and Weckhuysen B M 2012 *Nat. Nanotechnol.* **7** 583